Journal of Power Sources 251 (2014) 215–221

Contents lists available at ScienceDirect

Journal of Power Sources

journal homepage: www.elsevier.com/locate/jpowsour

Dye-sensitized solar cells with nanoporous TiO_2 photoanodes sintered by N_2 and air atmospheric pressure plasma jets with/without air-quenching

Haoming Chang [a], Chun-Ming Hsu [b], Peng-Kai Kao [b], Yao-Jhen Yang [b], Cheng-Che Hsu [b,1], I-Chun Cheng [c,2], Jian-Zhang Chen [a,*]

[a] Graduate Institute of Applied Mechanics, National Taiwan University, Taipei 10617, Taiwan
[b] Department of Chemical Engineering, National Taiwan University, Taipei 10617, Taiwan
[c] Graduate Institute of Photonics and Optoelectronics & Department of Electrical Engineering, National Taiwan University, Taipei 10617, Taiwan

HIGHLIGHTS

- DSSCs with TiO_2 sintered by N_2 and air APPJs with/without air-quenching.
- Air-quenching lowers the APPJ temperature from ~500 °C to ~300 °C.
- With air-quenching, the APPJ sintering time and temperature can be further reduced.
- 30-s ~300 °C APPJ TiO_2 sintering can replace conventional 510 °C × 15 min process.
- The DSSCs with APPJ sintered TiO_2 photoanodes exhibit comparable cell efficiency.

GRAPHICAL ABSTRACT

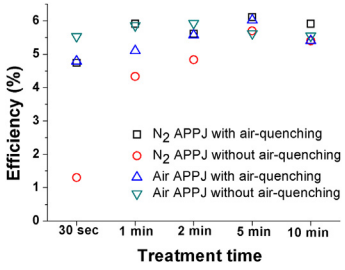

ARTICLE INFO

Article history:
Received 23 September 2013
Received in revised form
9 November 2013
Accepted 15 November 2013
Available online 28 November 2013

Keywords:
Atmospheric pressure plasma jets
Titania
Nanoporous materials
Sintering
Air-quenching

ABSTRACT

We investigate dye-sensitized solar cells (DSSCs) with TiO_2 photoanodes sintered by N_2 and air atmospheric pressure plasma jets (APPJs) with/without air-quenching. Air-quenching reduces the APPJ temperature from ~500 °C to ~300 °C; however, it accelerates the removal of organic solvents and the TiO_2 sintering process. N_2 APPJ with air-quenching and air APPJ with/without air-quenching can complete the sintering process in an ultra-short time (30 s); the assembled cells show efficiencies comparable to those of cells fabricated using conventional furnace process. The presence of excited nitrogen plasmas and oxygen gas is critical to the rapid sintering process of nanoporous TiO_2 photoanodes at a lower temperature (~300 °C). This air-quenched APPJ may be applied to the sintering process on lower-melting-point flexible substrate, which facilitates the future application to roll-to-roll process.

1. Introduction

Nanoporous materials have attracted much attention resulting from their particular properties and versatile applications [1,2]. The large surface/volume ratio and the nanoscale size effects of nanoporous materials result in unique properties that are not found in

* Corresponding author. Graduate Institute of Applied Mechanics, National Taiwan University, No.1 Sec. 4 Roosevelt Rd., Taipei City 10617, Taiwan. Tel./fax: +886 2 3366 5694.
E-mail addresses: chsu@ntu.edu.tw (C.-C. Hsu), iccheng@ntu.edu.tw (I.-C. Cheng), jchen@ntu.edu.tw (J.-Z. Chen).
[1] Department of Chemical Engineering, National Taiwan University, No.1 Sec. 4 Roosevelt Rd., Taipei City 10617, Taiwan. Tel.: +886 2 3366 3034; fax: +886 2 2362 3040.
[2] Graduate Institute of Photonics and Optoelectronics, Department of Electrical Engineering, National Taiwan University, No.1 Sec. 4 Roosevelt Rd., Taipei City 10617, Taiwan. Tel./fax: +886 2 3366 9648.

0378-7753/$ – see front matter © 2013 Elsevier B.V. All rights reserved.
http://dx.doi.org/10.1016/j.jpowsour.2013.11.051

the corresponding bulk materials [1,3,4]. Hence, nanoporous materials are extensively applied in various fields; they have been used as catalysts [5,6], for splitting water [7–9], as adsorbents [5,10], for gas storage [11], and in gas sensors [12], batteries [13,14], fuel cells [15], and photovoltaic cells [3,16,17]. Synthetic routes for nanoporous materials generally require templates [5,18,19], yet some template-free methods also have been developed [14]. This manuscript reports a rapid nanoporous TiO_2 fabrication process using an atmospheric pressure plasma jet (APPJ) with air-quenching. The nanoporous TiO_2 thus prepared was subsequently used as the photoanode of dye-sensitized solar cells (DSSCs) to demonstrate its practical application.

In 1991, O'Regan and Grätzel greatly improved the power conversion efficiency of DSSCs to 7.1% [20]. Subsequently, numerous studies have focused on this technology [21]. Through the implementation of new dyes, the DSSC efficiency was improved to 11% in 2005 [9], 11.5% in 2009 [22] and 13.1% in 2011 [23]. DSSCs are eco-friendly and cost effective; they can be fabricated without using expensive vacuum deposition systems. These features make DSSCs a potential alternative to conventional solar cells. In DSSCs, separate materials are used for light absorption and carrier transport. Organic dyes are optically excited to generate photoelectrons that are injected into the photoanodes and transported into the external load. Nanoporous materials are frequently used as photoanodes in DSSCs to increase the effective surface area for dye-anchoring [20]. Techniques such as electrophoretic deposition with post compression have been developed to fabricate nanoporous photoanodes of DSSCs on low-melting-point substrates [24]. However, thermal sintering still offers better connectivity among nanoparticles to reduce the photoelectron transport resistance. A typical nanoporous TiO_2 photoanode is usually fabricated by sintering TiO_2 nanoparticle pastes using a conventional furnace at 450–510 °C [25,26] for 15–30 min (excluding the heating and cooling periods). The thermal sintering process requires a long processing time with large thermal budget. Therefore, several alternative techniques have been developed to lower the cost and to shorten the energy payback time, for examples, microwave radiation [27], UV treatment [28], near infrared heating [29], dielectric barrier discharge [30], laser sintering [31], and atmospheric pressure plasma jet (APPJ) sintering [16].

APPJs possess large-area processing capability and have been applied to various material processes without requiring the use of expensive vacuum systems, for examples, oxide thin-film deposition [32], surface modification [33], surface cleaning [34,35], rapid annealing process for electronic heterostructure [36], and bio-medical treatments [37]. The energetic excited molecules in APPJs provide additional energy to assist the thermal process, thus offering rapid process capability [16,36]. In our previous study, we have successfully demonstrated that DSSCs fabricated using N_2 APPJs without air-quenching processes exhibited efficiencies comparable to those of conventional furnace processes; the TiO_2 sintering time was reduced to 1 min. In this study, we apply N_2 and air APPJs with/without air-quenching to sinter TiO_2 photoanodes. The APPJ sintering temperature can be reduced from ~500 °C to ~300 °C by air-quenching, whereas the processing time can be further reduced to 30 s. This can be achieved by air APPJ with/without air-quenching as well as by N_2 APPJ with air-quenching. The participation of oxygen in the reaction is the key for the success of this low temperature rapid sintering technique. The lower sintering temperature can facilitate the future application of this technique to flexible roll-to-roll processes using a lower-melting-point substrate; the substrate conveying speed can be increased owing to the ultra-short sintering time.

2. Experimental details

A nanoporous TiO_2 layer (E-solar P300, Everlight Chemical Industrial Co.) was deposited on the fluorine-doped tin-oxide-coated glass (FTO, TEC7, thickness: 2.2 mm, transmittance: >80%, sheet resistance: 8 $\Omega\ \square^{-1}$, Pilkington) by the screen-printing method. Screen-printing was repeated three times until the thickness of the nanoporous TiO_2 layer reached ~10 μm with an active area of 0.22 cm^2. The nanoporous TiO_2 layer was heated at 100 °C for 10 min (soft baking) after each screen-printing step to dry off the solvent. The film was then sintered by a N_2 (purity: 99.999%) or air (mixture gas, 79% N_2 + 21% O_2, purity: 99.995%) APPJ for 30 s, 1 min, 2 min, 5 min, and 10 min. The APPJ operating conditions are as follows: 35 slm gas flow, 275 V applied voltage, and 7/33 μs on/off duty cycle. The schematic of the APPJ system is shown in Fig. 1. The TiO_2 layer was located on a stage that was moved toward the APPJ with a velocity of 6 cm min^{-1}. The stage was moved forward for around 1 min, and the film was sintered for the specified durations under the plasma jet; then, the stage was moved backward with the same velocity after the sintering process. A 2-cm-long quartz with a 1.7-cm-diameter side hole was used to perform the air-quenching. A comparative experiment was conducted with the side hole being sealed with a Kapton tape such that the air-quenching effect was stopped. The temperature evolution was monitored using a K-type thermocouple in contact with the substrate during APPJ operations. The data were acquired by a data acquisition device (USB-6221, National Instruments) using a computer. The steady-state temperatures of the operating conditions are listed in Table 1. Air-quenching significantly reduced the APPJ temperatures. More details regarding the APPJ system used in this study have been provided in other literature [32,38,39].

After sintering, the TiO_2 nanoporous film was submerged in a mixed solution of acetonitrile (99.9%, J. T. Baker) and tertiary butyl alcohol (99.9%, J. T. Baker) containing 3×10^{-4} M of N719 dye (Solaronix) for 24 h. The dye-adsorbed TiO_2 films were further rinsed with ethanol and dried in air. The photoanode was then assembled with the counter electrode of a sputtered 10-nm-thick Pt layer on the FTO glass substrate. Finally, a liquid electrolyte (Eversolar EL 100, Everlight Chemical Industrial Co.), consisting of I_2, LiI, guanidinium thiocyanate (GuNCS) and acetonitrile, was injected into the assembled cells.

The optical emission spectra (OES) emanating from the plasma were monitored using a spectrometer (Princeton Instruments, SP2500i) to probe the semi-quantitative information associated with the reactive species. A UV–Vis–NIR spectrophotometer (JASCO V-670) was used to determine the absorption spectra of nanoporous TiO_2 layers. The absorption was calculated by the formula $A = 1 - T - R$, where A is the absorption; T, the transmission; R, the reflection. Both T and R were measured using an integral sphere. The surface elemental composition was determined by X-ray photoelectron spectroscopy (XPS, VG ESCA Scientific Theta Probe). For the power efficiency measurements of the DSSCs, the cells were illuminated through the FTO glass substrate using a solar simulator (WACOM, WXS-155S-L2) with an AM1.5 filter. A Keithley 2400 electrometer was used to evaluate the I–V characteristics. Electrochemical impedance spectroscopy (EIS) analysis was performed using an electrochemical workstation (Zahner Zennium). The EIS spectra were obtained by applying sinusoidal perturbations of ±10 mV with a frequency of 0.1–10^5 Hz at the open circuit voltage (V_{oc}) under the illumination of a solar simulator.

3. Results and discussion

To identify reactive species that are generated in the N_2 and air APPJs, the emission spectra were recorded from 200 to 800 nm

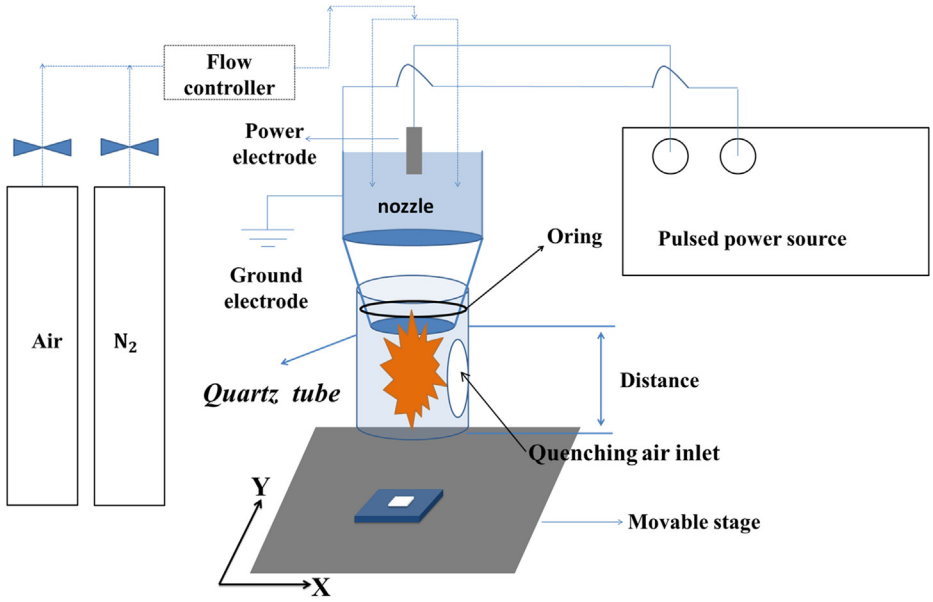

Fig. 1. Schematic of APPJ apparatus.

using a spectrometer. The spectra are shown in Fig. 2. In N_2 APPJ, the N_2 1st positive $B^3\Pi_g \rightarrow A^3\Sigma_u^+$ and 2nd positive $C^3\Pi_u \rightarrow B^3\Pi_g$ can be clearly observed in Fig. 2(a) [38,39]. These emissive signals associated with the excited N_2 molecules are reduced when ambient air is introduced through the side hole to quench the APPJ. The air-quenching reduces the electron number density of the N_2 APPJ owing to the higher electron affinity of oxygen, which in turn reduces the highly energetic excited N_2 molecules. When ambient air is introduced to the N_2 APPJ, the emissive signal intensities of the NO-β transition $B^2\Pi \rightarrow X^2\Pi$ and NO-γ transition $A^2\sum^+ \rightarrow X^2\Pi$ increase in the shorter wavelength region, suggesting that oxygen from ambient air reacts with the N_2 APPJ to form some NO molecules [34]. Fig. 2(b) shows the OES of air APPJs. Emissions from the O radicals (777 nm) and hydroxide radicals (−OH) are identified in Fig. 2(b), but no other emissive reactions are observed. In addition, a broad continuum centered at ~650 nm is observed. The origin of such an emission has not yet been identified. Various mechanisms may produce this emission, such as thermal emission and molecular emission caused by chemiluminescent reactions [40].

Fig. 3(a) shows the absorption spectra of nanoporous TiO_2 layers treated by N_2 APPJ. The TiO_2 layers sintered with air-quenched APPJ show similar absorption spectra. However, 30-s APPJ sintered TiO_2 without air-quenching shows an extra absorption tail in the wavelength range from 350 to 600 nm. The 30-s sintered film appears brown owing to the incomplete removal of the organic solvent which results in an extra absorption [28,30]. When the APPJ sintering time exceeds 1 min, the absorption spectra are almost identical to each other. Fig. 3(b) shows the absorption spectra of TiO_2 sintered by air APPJ. All spectra are similar for TiO_2 sintered by air APPJs with/without air-quenching. This strongly suggests that the involvement of oxygen in the APPJ-TiO_2 reaction facilitates the removal of organic solvents.

Table 1
Steady-state surface temperatures during APPJ treatments.

	With air-quenching (no tape)	Without air-quenching (taped)
N_2 APPJ	320 °C	430 °C
Air APPJ	340 °C	470 °C

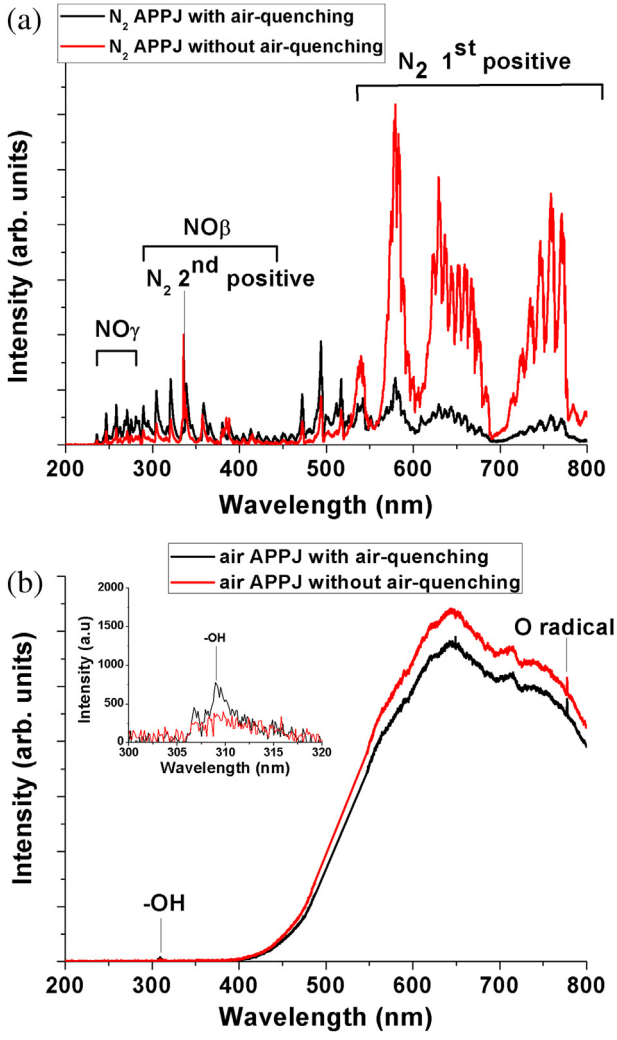

Fig. 2. OES of the APPJs with/without air-quenching. (a) N_2 plasma, (b) air plasma.

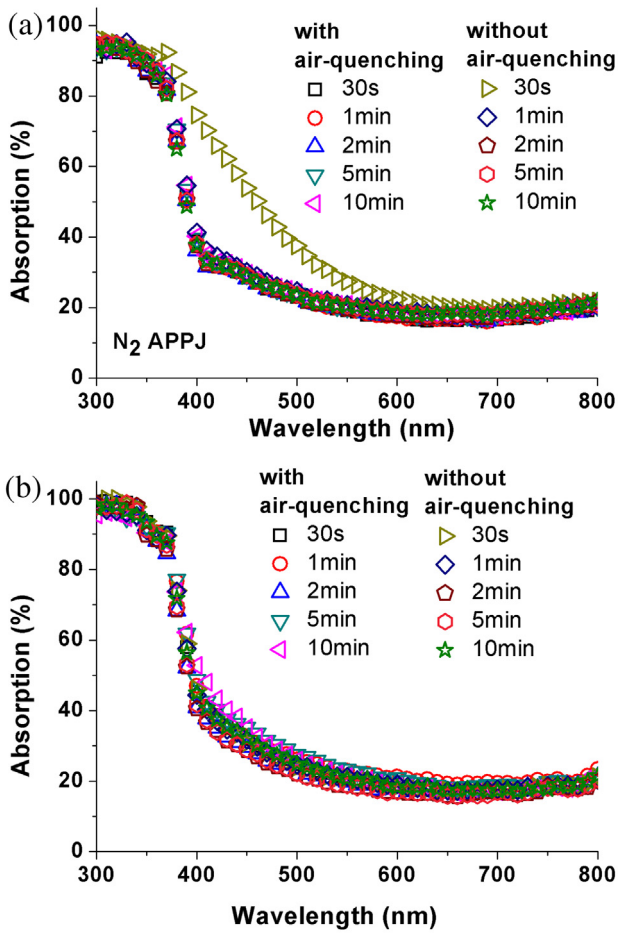

Fig. 3. UV–visible spectra of pure TiO_2 with (a) N_2 treatment and (b) Air treatment.

Fig. 4 shows the power conversion efficiency as a function of APPJ sintering time. The detailed cell parameters are listed in Table 2. Except for cells with TiO_2 treated by N_2 APPJ without air-quenching, all the assembled cells exhibit comparable efficiencies. The cell with a TiO_2 photoanode sintered by N_2 APPJ without air-quenching for 30 s shows extremely low efficiency, photocurrent density, open circuit voltage, and fill factor because

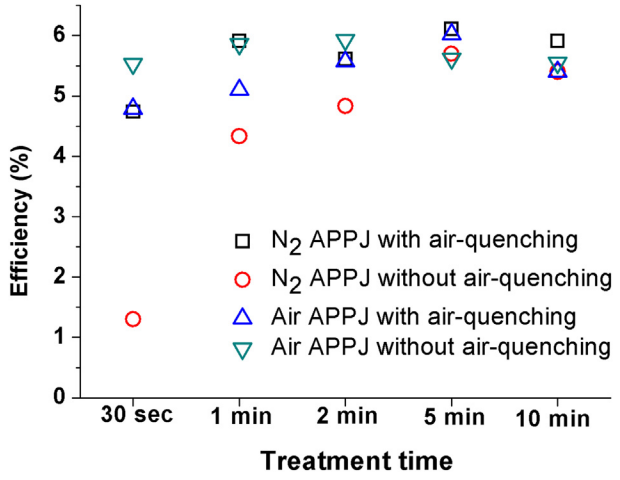

Fig. 4. Power conversion efficiency of DSSCs measured under AM1.5, 100 mW cm^{-2} illumination.

Table 2
Cell performance in this study.

APPJ	Carrier gas	Air-quenching	J_{sc} (mA cm^{-2})	V_{oc} (V)	F.F	Efficiency (%)
30 s	N_2	Yes	9.21	0.748	0.687	4.74
1 min	N_2	Yes	11.3	0.755	0.692	5.91
2 min	N_2	Yes	11.1	0.759	0.665	5.61
5 min	N_2	Yes	12.1	0.753	0.669	6.11
10 min	N_2	Yes	12.1	0.747	0.654	5.91
30 s	N_2	No	2.97	0.638	0.684	1.30
1 min	N_2	No	8.62	0.747	0.674	4.33
2 min	N_2	No	8.92	0.770	0.704	4.83
5 min	N_2	No	10.8	0.762	0.693	5.70
10 min	N_2	No	10.2	0.768	0.685	5.40
30 s	Air	Yes	9.46	0.748	0.677	4.79
1 min	Air	Yes	10.2	0.744	0.672	5.10
2 min	Air	Yes	10.8	0.771	0.668	5.57
5 min	Air	Yes	12.1	0.741	0.672	6.02
10 min	Air	Yes	10.5	0.767	0.669	5.40
30 s	Air	No	10.8	0.746	0.677	5.53
1 min	Air	No	11.3	0.751	0.672	5.86
2 min	Air	No	11.3	0.762	0.668	5.93
5 min	Air	No	10.8	0.760	0.685	5.62
10 min	Air	No	11.0	0.761	0.662	5.55

of the incomplete removal of organic substances, which is consistent with the results of the absorption spectra. The cells with TiO_2 sintered by N_2 APPJ without air-quenching require a longer sintering time to achieve power conversion efficiency comparable to those of other cells. This suggests that the involvement of oxygen can accelerate the removal of organic solvents and the sintering process. We have also attempted to sinter TiO_2 with pure O_2 APPJ; however, a strong reaction occurs in the stainless steel jet and results in sample contamination with small steel particles. The TiO_2 sintering time (30 s) is extremely short compared to that using a conventional furnace (15 min excluding heating and cooling time) [16]. The ultra-short sintering time is attributed to the synergistic effect of the temperature and the reactivity of the APPJs. For N_2 APPJs, the excited nitrogen molecules possess energy over 6 eV above the ground state, compared to 1–2 eV in the case of oxygen molecules. These highly energetic molecules facilitate the dissociations of organic solvents. This rapid processing is made possible by the reaction of excited nitrogen molecules and dissociated oxygen species. Air-quenching significantly lowers the N_2 and air APPJs to 320 °C and 340 °C, respectively; nevertheless, the DSSCs with TiO_2 sintered by 30-s air-quenched N_2/air APPJs show comparable cell efficiencies. This indicates that the introduction of oxygen can lower the APPJ temperature such that this process may be used for sintering on a lower-melting-point substrate. This also suggests that the energetic plasmas indeed enhance the sintering to shorten the processing time. All these results strongly suggest that APPJ processed DSSCs can achieve efficiencies comparable to those of DSSCs fabricated by conventional processes with an ultra-short processing time (<30 s) and low temperature (~300 °C).

Fig. 5 shows the Nyquist plots of the EIS results for DSSCs under 100 mW cm^{-2} light illumination. The model of the equivalent circuit is presented elsewhere [41] and the experimental data of impedance spectra are fitted by the *Z*-view software (Scribner Associates, Inc.). Typically, the plot shows three semicircles, corresponding to the resistance of the Pt/electrolyte and TiO_2/dye/electrolyte interfaces as well as the Warburg diffusion process of I^-/I_3^- [42]. The first semicircle in the high-frequency region corresponds to the Pt/electrolyte interface because its metallic characteristic has the smallest resistance R_{ct1} in DSSC. The middle semicircle represents the TiO_2/dye/electrolyte interface, and the

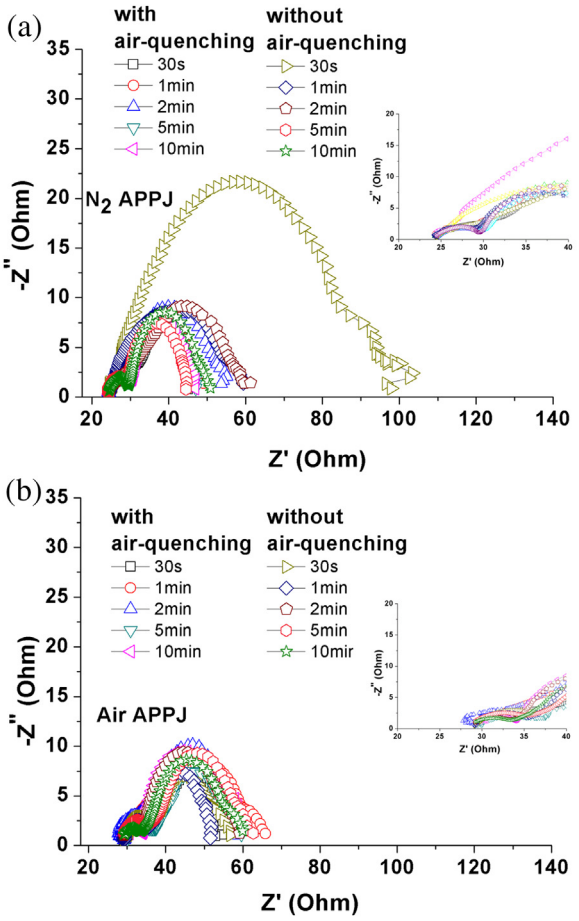

Fig. 5. Nyquist plots of DSSCs with TiO_2 photoanodes sintered by (a) N_2 and (b) air APPJs.

circle diameter represents the value of the impedance R_{ct2}. The values of constant phase elements (CPE) are also estimated from the fitting curve by *Z*-view. The CPE is a non-intuitive circuit element that is invented while examining the response of the complicated electrochemical impedance system. The CPE is expressed by the equation $Z = [1/Q(j\omega)^{\alpha}]$ with two parameters Q ($\Omega^{-1}s^{\alpha}$ cm^{-2}) and α (dimensionless), which respectively denote the false capacitance and non-homogeneity constant [43]. The fitting results for various experimental conditions are listed in Table 3. The comparisons of cell efficiency, R_{ct2}, Q, and α are plotted in Fig. 6.

In the case of N_2 APPJs without air-quenching, the cell efficiency increases with the increase in Q and α and the decrease in R_{ct2}, as shown in Fig. 6(a) and (b). The efficiency gradually increases as the APPJ sintering time increases from 30 s to 2 min and then levels off; R_{ct2} shows a corresponding falling trend, whereas Q and α reveal rising trends. The cell with TiO_2 sintered for 30 s shows extremely high R_{ct2} and lower Q and α, which is attributed to the incomplete removal of the organic substance in the TiO_2 paste. The cell efficiency increases with the increase in Q and α, and the decrease in R_{ct2} as the treatment time increases to 2 min. These values are maintained at similar levels with a further increase in sintering time. Lower Q and α suggest that the films have poor porosity or smaller active area owing to the incomplete conversion of TiO_2 pastes into nanoporous TiO_2 networks [44,45]. In contrast, no significant differences are observed in efficiency, R_{ct2}, Q and α with the air APPJ sintering time, as shown in Fig. 6(c) and (d). N_2 APPJ with air-quenching and air APPJ with/without air-quenching can sinter

Table 3
EIS parameters extracted from Fig. 6.

APPJ	Carrier gas	Air-quenching	Efficiency (%)	R_{ct2} (Ω)	Q (10^{-3} Ω^{-1} s^{α} cm^{-2})	α (dimensionless)
30 s	N_2	Yes	4.74	17.8	4.6	0.908
1 min	N_2	Yes	5.91	14.2	5.0	0.936
2 min	N_2	Yes	5.61	15.3	4.9	0.917
5 min	N_2	Yes	6.11	14.0	4.9	0.976
10 min	N_2	Yes	5.91	16.1	4.9	0.927
30 s	N_2	No	1.30	61.5	1.7	0.583
1 min	N_2	No	4.33	35.2	3.8	0.596
2 min	N_2	No	4.83	21.9	3.9	0.663
5 min	N_2	No	5.70	14.5	4.5	0.981
10 min	N_2	No	5.40	18.1	4.3	0.934
30 s	Air	No	4.79	15.1	4.7	0.886
1 min	Air	No	5.10	20.4	5.6	0.905
2 min	Air	No	5.57	18.2	5.8	0.906
5 min	Air	No	6.02	16.1	6.0	0.905
10 min	Air	No	5.40	19.8	4.5	0.945
30 s	Air	Yes	5.53	16.9	5.8	0.945
1 min	Air	Yes	5.86	15.7	6.8	0.903
2 min	Air	Yes	5.93	16.2	5.2	0.926
5 min	Air	Yes	5.62	19.8	4.0	0.892
10 min	Air	Yes	5.55	19.0	4.3	0.901

TiO_2 more efficiently. The involvement of oxygen in the APPJ can enhance the removal of organic solvents in TiO_2 pastes, which makes ultra-short TiO_2 sintering time possible at lower temperatures.

The effects of APPJs on sintered TiO_2 films result primarily from the synergy between the thermal effect (temperature) and the chemical reactivity. The calcination process for screen-printed TiO_2 films requires the removal of the organic compounds (e.g., solvent and binder) as well as the sintering of TiO_2 nanoparticles. Treatment by APPJs with air-quenching requires an ultra-short treatment time (30 s) for the cell to achieve conversion efficiency greater than 4.5%, regardless of the fact that the APPJ exhibits a lower temperature (below 350 °C, as indicated in Table 1). In the case of the treatment by the N_2 APPJ without air-quenching, the jet temperature is 430 °C and a 1 or 2 min treatment time is necessary to achieve an efficiency of 4.33% and 4.83%, respectively (Table 2). The UV–Vis spectrum (Fig. 3) demonstrates incomplete removal of organic compounds with 30 s of treatment. This observation indicates that the existence of oxygen-containing reactive species (e.g., O radical and O_3) plays a key role in the ultra-fast treatment for organic compound removal when oxygen is introduced to the APPJ. This is consistent with the results reported by Chiang et al. [34]. The effect of the existence of oxygen-containing reactive species dominates over that of the lower APPJ temperature in removal rates of organic compounds. The substrate temperature of TiO_2 calcination by APPJ with air-quenching (320 °C) is lower than that of conventional thermal annealing processes (450 °C or greater). A DSSC conversion efficiency of greater than 4.5% with an ultra-short treatment time (30 s) strongly suggests that the APPJ is capable of effective TiO_2 calcination at a lower temperature due to the synergetic effect of the temperature and the chemical reactivity of the APPJ.

The original installation of the glass tube in the N_2 APPJ was designated for air entrainment minimization, which prevented the quenching of excited nitrogen molecules by oxygen and yielded higher excited nitrogen molecule densities, as indicated in our previous work [38,39]. Such an approach shows a significant increase in the effective treated area for glass surface treatment [39]. The introduction of air (oxygen) is capable of effectively sintering screen-printed TiO_2 films, despite the reduction in excited state nitrogen molecule densities. This observation is significant for the process flexibility and the APPJ capacity, allowing for the APPJ to be used in broader applications.

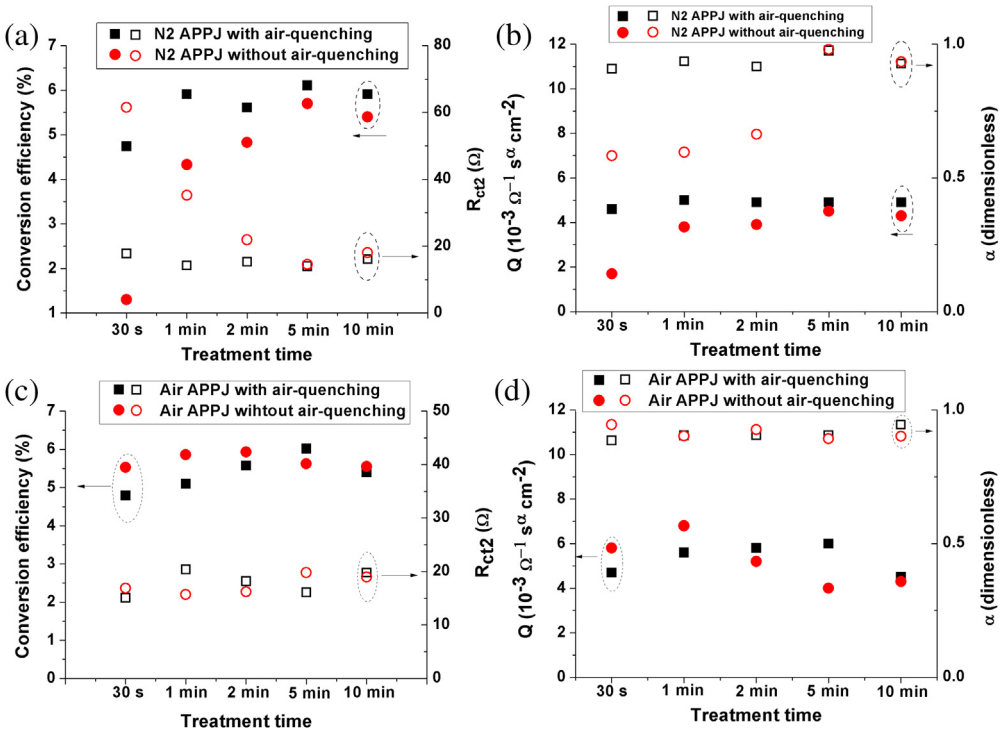

Fig. 6. Plots of efficiency and EIS parameters for DSSCs with TiO_2 sintered by (a)(b) N_2 APPJs and (c)(d) air APPJs.

4. Conclusion

We investigated DSSCs with TiO_2 photoanodes sintered by N_2 and air APPJ with/without air-quenching. The introduction of ambient air reduced the APPJ temperatures; however, the involvement of oxygen in the APPJ facilitated the removal of organic solvents and accelerated the sintering process. N_2 APPJ with air-quenching and air APPJ with/without air-quenching can complete the sintering process in an ultra-short time (30 s), and the assembled cells showed efficiency comparable to that of the conventional furnace process. The presence of excited nitrogen plasmas and oxygen gas was critical to the rapid sintering process of nanoporous TiO_2 photoanodes. The rapid APPJ TiO_2 sintering temperature was reduced to ~300 °C with air-quenching, in comparison to the value of ~500 °C previously published by our group. This facilitates the future use of this APPJ sintering on lower-melting-point flexible substrate. This is beneficial for roll-to-roll fabrication processes. The thermal budget and energy required for the DSSC fabrication process are also lowered.

Acknowledgments

This research was funded by the Center for Emerging Material and Advanced Devices, National Taiwan University. The authors also gratefully acknowledge funding support from the National Science Council of Taiwan under grant nos. NSC 102-2221-E-002-060, NSC 101-2628-E-002-020-MY3, and NSC 102-3113-P-002-027.

References

[1] A. Corma, Chem. Rev. 97 (1997) 2373–2419.
[2] M.E. Davis, Nature 417 (2002) 813–821.
[3] A. Corma, P. Atienzar, H. Garcia, J.Y. Chane-Ching, Nat. Mater. 3 (2004) 394–397.
[4] S. Forster, T. Plantenberg, Angew. Chem. Int. Ed. 41 (2002) 689–714.
[5] L.S. Zhong, J.S. Hu, L.J. Wan, W.G. Song, Chem. Commun. (2008) 1184–1186.
[6] L.X. Hou, H.J. Qiu, J. Power Sources 216 (2012) 28–32.
[7] T. Sreethawong, C. Junbua, S. Chavadeja, J. Power Sources 190 (2009) 513–524.
[8] T.Y. Peng, D.N. Ke, P. Cai, K. Dai, L. Ma, L. Zan, J. Power Sources 180 (2008) 498–505.
[9] M. Gratzel, Chem. Lett. 34 (2005) 8–13.
[10] M. Pena, X.G. Meng, G.P. Korfiatis, C.Y. Jing, Environ. Sci. Technol. 40 (2006) 1257–1262.
[11] R.E. Morris, P.S. Wheatley, Angew. Chem. Int. Ed. 47 (2008) 4966–4981.
[12] L.G. Teoh, Y.M. Hon, J. Shieh, W.H. Lai, M.H. Hon, Sens. Actuator B-chem. 96 (2003) 219–225.
[13] W.Y. Li, L.N. Xu, J. Chen, Adv. Funct. Mater. 15 (2005) 851–857.
[14] Y.G. Guo, Y.S. Hu, J. Maier, Chem. Commun. (2006) 2783–2785.
[15] C.H. Ko, K. Kerman, S. Ramanathan, J. Power Sources 213 (2012) 343–349.
[16] H. Chang, Y.-J. Yang, H.-C. Li, C.-C. Hsu, I. Cheng, J.-Z. Chen, J. Power Sources 234 (2013) 16–22.
[17] M.M. Lee, J. Teuscher, T. Miyasaka, T.N. Murakami, H.J. Snaith, Science 338 (2012) 643–647.
[18] P.D. Yang, D.Y. Zhao, D.I. Margolese, B.F. Chmelka, G.D. Stucky, Nature 396 (1998) 152–155.
[19] Y.Y. Wu, G.S. Cheng, K. Katsov, S.W. Sides, J.F. Wang, J. Tang, G.H. Fredrickson, M. Moskovits, G.D. Stucky, Nat. Mater. 3 (2004) 816–822.
[20] B. O'regan, M. Grfitzeli, Nature 353 (1991) 24.
[21] M. Grätzel, Prog. Photovolt. Res. Appl. 14 (2006) 429–442.
[22] C.Y. Chen, M.K. Wang, J.Y. Li, N. Pootrakulchote, L. Alibabaei, C.H. Ngoc-le, J.D. Decoppet, J.H. Tsai, C. Gratzel, C.G. Wu, S.M. Zakeeruddin, M. Gratzel, ACS Nano 3 (2009) 3103–3109.
[23] A. Yella, H.W. Lee, H.N. Tsao, C.Y. Yi, A.K. Chandiran, M.K. Nazeeruddin, E.W.G. Diau, C.Y. Yeh, S.M. Zakeeruddin, M. Gratzel, Science 334 (2011) 629–634.
[24] H.W. Chen, C.Y. Lin, Y.H. Lai, J.G. Chen, C.C. Wang, C.W. Hu, C.Y. Hsu, R. Vittal, K.C. Ho, J. Power Sources 196 (2011) 4859–4864.
[25] Y.G. Seo, K. Woo, J. Kim, H. Lee, W. Lee, Adv. Funct. Mater. 21 (2011) 3094–3103.
[26] D.-W. Liu, I. Cheng, J.Z. Chen, H.-W. Chen, K.-C. Ho, C.-C. Chiang, Opt. Express 20 (2012) A168–A176.
[27] S. Uchida, M. Tomiha, N. Masaki, A. Miyazawa, H. Takizawa, Sol. Energy Mater. Sol. Cells 81 (2004) 135–139.
[28] L.N. Lewis, J.L. Spivack, S. Gasaway, E.D. Williams, J.Y. Gui, V. Manivannan, O.P. Siclovan, Sol. Energy Mater. Sol. Cells 90 (2006) 1041–1051.
[29] T. Watson, I. Mabbett, H. Wang, L. Peter, D. Worsley, Prog. Photovolt. Res. Appl. 19 (2011) 482–486.
[30] S. Zen, Y. Teramoto, R. Ono, T. Oda, Jpn. J. Appl. Phys. 51 (2012) 6201.
[31] G. Mincuzzi, L. Vesce, A. Reale, A. Di Carlo, T.M. Brown, Appl. Phys. Lett. 95 (2009) 103312.
[32] Y.-w. Hsu, H.-C. Li, Y.-J. Yang, C.-c. Hsu, Thin Solid Films 519 (2011) 3095–3099.
[33] J. Sun, L. Yao, Z. Gao, S. Peng, C. Wang, Y. Qiu, Surf. Coat. Technol. 204 (2010) 4101–4106.

[34] M.-H. Chiang, K.-C. Liao, I.-M. Lin, C.-C. Lu, H.-Y. Huang, C.-L. Kuo, J.-S. Wu, C.-C. Hsu, S.-H. Chen, Plasma Chem. Plasma Process. 30 (2010) 553–563.
[35] T. Homola, J. Matoušek, V. Medvecká, A. Zahoranová, M. Kormunda, D. Kováčik, M. Černák, Appl. Surf. Sci. 258 (2012) 7135–7139.
[36] S.T. Lien, H.C. Li, Y.J. Yang, C.C. Hsu, I.C. Cheng, J.Z. Chen, J. Phys. D Appl. Phys. 46 (2013) 075202.
[37] J. Young Kim, D.-H. Lee, J. Ballato, W. Cao, S.-O. Kim, Appl. Phys. Lett. 101 (2012) 224101–224105.
[38] Y.-w. Hsu, Y.-j. Yang, C.-y. Wu, C.-c. Hsu, Plasma Chem. Plasma Process. 30 (2010) 363–372.
[39] C.-C. Hsu, Y.-J. Yang, IEEE Trans. Plasma Sci. 38 (2010) 496–499.
[40] V.M. Donnelly, D.L. Flamm, J. Appl. Phys. 51 (1980) 5273–5276.
[41] K.-M. Lee, V. Suryanarayanan, K.-C. Ho, Sol. Energy Mater. Sol. Cells 91 (2007) 1416–1420.
[42] C.-P. Hsu, K.-M. Lee, J.T.-W. Huang, C.-Y. Lin, C.-H. Lee, L.-P. Wang, S.-Y. Tsai, K.-C. Ho, Electrochim. Acta 53 (2008) 7514–7522.
[43] Y.H. Chen, K.C. Huang, J.G. Chen, R. Vittal, K.C. Ho, Electrochim. Acta 56 (2011) 7999–8004.
[44] M.X. Wu, X. Lin, T.H. Wang, J.S. Qiu, T.L. Ma, Energy Environ. Sci. 4 (2011) 2308–2315.
[45] G.H. Liu, H. Wang, X. Li, Y.G. Rong, Z.L. Ku, M. Xu, L.F. Liu, M. Hu, Y. Yang, P. Xiang, T. Shu, H.W. Han, Electrochim. Acta 69 (2012) 334–339.